Influence of typology and management practices on water pCO 2 and atmospheric CO2 fluxes over two temperate shelf–estuary–marsh water continuums

Jérémy Mayen, Pierre Polsenaere, Aurore Regaudie de Gioux, Christine Dupuy, Marie Vagner, Jean-Christophe Lemesle, Benoit Poitevin, Philippe Souchu

Influence of typology and management practices on water pCO_2 and atmospheric CO_2 fluxes over two temperate shelf – estuary – marsh water continuums

Jérémy Mayen[1,2*], Pierre Polsenaere[1], Aurore Regaudie De Gioux[3], Christine Dupuy[4], Marie Vagner[5], Jean-Christophe Lemesle[6], Benoit Poitevin[7], Philippe Souchu[2]

*Corresponding author: jeremy.mayen@ifremer.fr

[1] IFREMER, Littoral, Laboratoire Environnement Ressources des Pertuis Charentais (LER-PC), BP 133, 17390, La Tremblade, France

[2] IFREMER, Littoral, Laboratoire Environnement Ressources Morbihan-Pays de Loire (LER-MPL), BP 21105, 44311, Nantes, France

[3] IFREMER, Dyneco, Pelagos, ZI de la Pointe du Diable - CS 10070 - 29280 Plouzané, France

[4] UMR 7266 Littoral Environnement et Société (LIENSs), CNRS – La Rochelle Université, France

[5] LEMAR, UMR 6539 CNRS/Univ Brest/IRD/Ifremer, ZI pointe du diable, 29 280, Plouzané, France

[6] LPO, Réserve Naturelle de Lilleau des Niges, 17880, Les Portes en Ré, France

[7] Pôle-Nature de l'Ecomusée du Marais Salant, route de Loix, 17111, Loix en Ré, France

A research paper submitted to the Regional Studies in Marine Science.

Abstract

Within the coastal zone, salt marshes often behave as atmospheric CO_2 sinks, allowing for blue carbon (C) sequestration associated with intense autotrophic metabolism. However, C dynamics over salt marshes are complex since various biogeochemical processes and fluxes take place at different terrestrial – aquatic – atmospheric exchange interfaces and spatiotemporal scales. This study focuses on seasonal, tidal and diurnal variations of water pCO_2, estimated water-air CO_2 fluxes and controlling factors along two temperate shelf – estuary – marsh continuums. The latter include typical coastal systems (shelf, estuary and channel) with artificial salt marshes that have contrasting management practices. Our high-frequency (seasonal 24-hour cycles) biogeochemical measurements at the various stations highlighted a strong control of ecosystem typology on inorganic C dynamics with lower water pCO_2 values in the artificial salt marshes, due to stronger biological activity and longer water residence times, than in the tidal estuary. In this marine-dominated estuary, water pCO_2 variations (267 - 569 ppmv) were strongly controlled by tidal effects and phytoplankton activity particularly in spring/summer. On the contrary, the greatest amplitudes in water pCO_2 were recorded in the artificial salt marshes (6 - 721 ppmv) due to intense macrophyte activity. However, in the rewilded artificial marsh, spring/summer fast-growing macroalgae produced, in turn, strong fall atmospheric CO_2 outgassing from degraded algae waters and thus a net annual source of CO_2 to the atmosphere (17.5 g C m^{-2} yr^{-1}). Conversely, management practices at the working artificial marsh for salt-farming activity with longer winter water residence times favoured rather slow-growing macrophytes which greatly contribute to the yearly observed atmospheric CO_2 sink (-97.7 g C m^{-2} yr^{-1}) and, more generally, blue C sequestration. We suggest that artificial salt marsh management can be used to control the contribution of primary producers to marsh C budget as atmospheric CO_2 (sink and/or source).

Key words: shelf – estuary – marsh continuums; water pCO_2; air-water CO_2 fluxes; diurnal, tidal, seasonal scales; marsh management practices; macrophytes.

Graphical Abstract

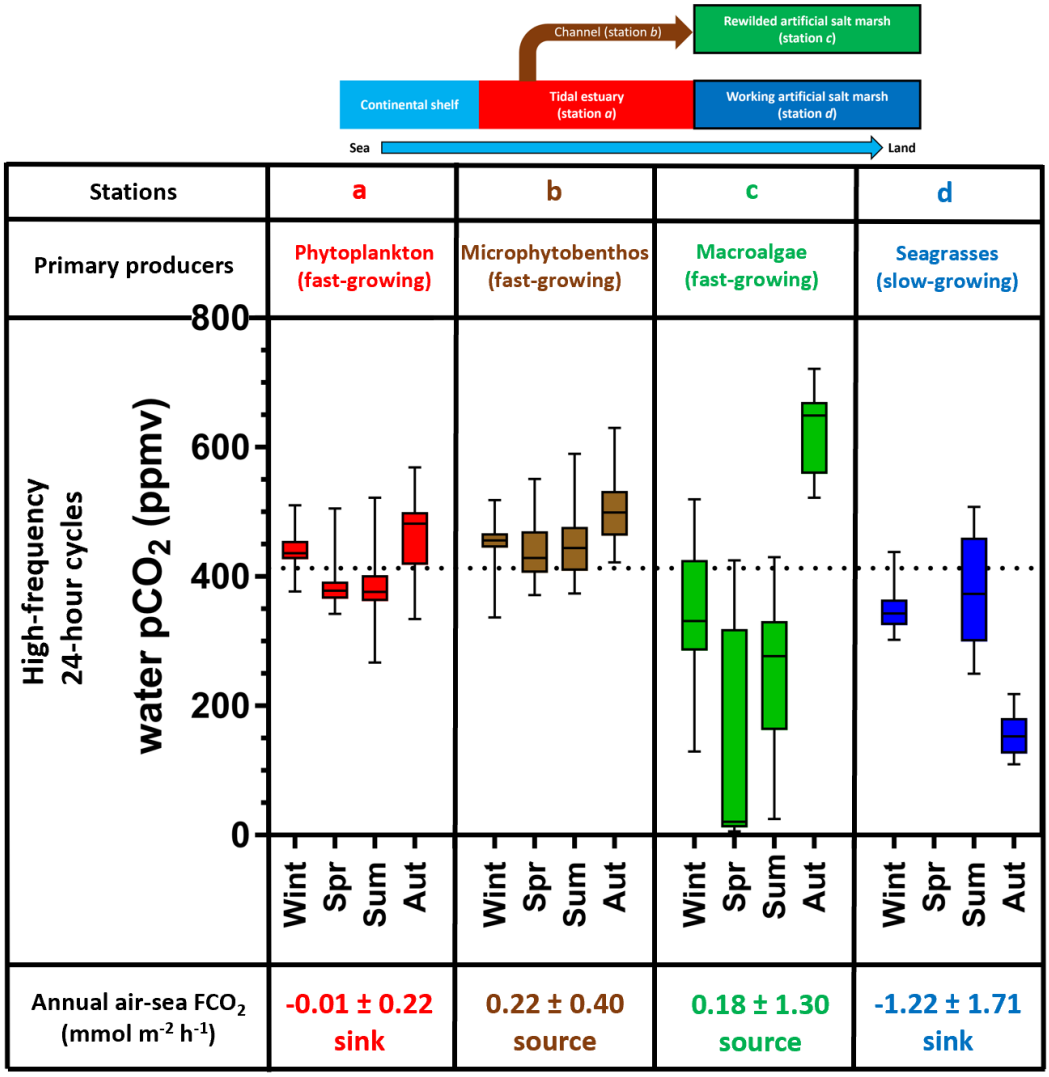

Water management practices and primary producer types influence the marsh CO_2 behaviour (sink/source)

1. Introduction

Marine coastal environments, which only account for 7% of the global ocean, perform major ecological functions such as primary production, bacterial mineralization, organic matter burial and calcium carbonate deposition (Gattuso et al. 1998). Comprised of mixed continental and oceanic waters, the coastal zone presents a wide diversity of geomorphological types and ecosystems (shelves, estuaries, bays, tidal wetlands) shaping the biogeochemical cycle coupling between the land, ocean and atmosphere (Aufdenkampe et al. 2011, Bauer et al. 2013). On the one hand, these dynamic and heterogeneous ecosystems behave as an active horizontal pipe carrying and processing large quantities of carbon (~0.90 ± 0.05 Pg C yr^{-1}, Cole et al. 2007) from the drainage basin to the open ocean (Cai 2011, Najjar et al. 2018). On the other hand, the coastal zone vertically exchanges large and variable quantities of carbon (C) with both the atmosphere and sediments (Cole et al. 2007, Polsenaere et al. 2012). For instance, at the global scale, continental shelves behave as atmospheric CO_2 sinks and absorb 0.25 ± 0.05 Pg C yr^{-1} (Bauer et al. 2013, Dai et al. 2022) due to phytoplankton primary production (Cloern et al. 2014). On the contrary, CO_2 supersaturated estuarine waters emit 0.25 ± 0.05 Pg C yr^{-1} to the atmosphere (Bauer et al. 2013) due to a high mineralization of organic matter from the land (Frankignoulle et al. 1998, Borges & Abril 2011). These atmospheric C exchanges within the coastal zone are heterogeneous (Borges et al. 2005) and need to be better taken into account in regional and global C budgets (Polsenaere 2011, Najjar et al. 2018). For instance, coastal wetlands, including salt marshes located along inner shelf – estuary – marsh continuums, absorb 0.55 ± 0.05 Pg C yr^{-1} from the atmosphere (Bauer et al. 2013) and may play a major role in atmospheric CO_2 uptake and associated organic C burial on Earth (Cai 2011, Mcleod et al. 2011).

In salt marshes, inorganic C dynamics and water pCO_2 in particular are influenced by several physicochemical and biological processes within and between each ecosystem compartment such as tidal exchanges, calcium carbonate precipitation/dissolution, benthic-pelagic couplings, air-water exchanges and photosynthesis/respiration balance (Cai 2011, Bauer et al. 2013, Macreadie et al. 2017). Due to high photoautotrophy rates of both aquatic (micro-algae and macrophytes) and terrestrial (vascular plants) primary producers, these highly productive ecosystems mostly behave as net atmospheric C sinks (Schäfer et al. 2014, Artigas et al. 2015, Forbrich & Giblin 2015). For instance, net primary production (NPP) values in *Spartina alterniflora* salt marshes ranged from 100 to > 2500 g C m^{-2} yr^{-1} (Duarte & Cebrián 1996, Tobias & Neubauer 2019) allowing for significant CO_2 uptake (Wang & Cai 2004). A refractory part of organic C produced through photosynthesis in these vegetated coastal ecosystems can then be largely sequestered in sediments (Chmura et al. 2003) and stored as blue C at a rate of 218 ± 24 g C m^{-2} yr^{-1}, and greatly contribute to the regional/global C cycle in comparison with terrestrial ecosystems (Mcleod et al. 2011). Salt marshes also produce and horizontally export significant quantities of C through tidal water advection (Najjar et al. 2018) which could, in turn, strongly influence the C balance of the system itself as well as the estuary and shelf systems (Cai 2011). The "marsh CO_2 pump" hypothesis proposes that atmospheric CO_2 fixation by plants and phytoplankton in marshes and the export of part of the associated C may be one of the major mechanisms making adjacent coastal waters sources of CO_2 to the atmosphere (Wang & Cai 2004). To illustrate this, Wang et al. (2016) used continuous in situ measurements of relevant biogeochemical parameters and water fluxes in an intertidal salt marsh in northeast region of the United States (12300 km^2) to estimate the total net CO_2 fixation (NPP) of 13.2 Tg C yr^{-1}. Of this total NPP value, 56% was exported to the coastal ocean through the outwelling phenomenon (horizontal advection) with inorganic and organic C accounting for

39% and 17%, respectively; this means that the export of C from marsh tides could represent a major proportion (414 g C m^{-2} yr^{-1}) in the overall marsh budget (Wang et al. 2016). Nevertheless, despite these major ecological potentials (storm protection, nursery areas, long-term C storage), these interface zones are the most threatened in the world by land-use changes, climate changes and sea level rise as described by Gu et al. (2018) in salt marshes in China. Moreover, coastal eutrophication causes the loss of salt marshes by decreasing the below-ground biomass of plant roots through microbial degradation thereby producing a decrease in the geomorphic stability of marshes (Deegan et al. 2012). Since the 1800s, salt marshes have lost about 25% of their global area with negative effects on the atmospheric CO_2 sink and the associated C sequestration (Mcleod et al. 2011). Their importance as ecosystem service reservoirs has made it possible to implement protection and restoration policies that contribute to their better management and to the development of their ecological and economic potentials (Gu et al. 2018, Adam 2019).

The high heterogeneity in biogeochemical processes within coastal systems at spatial and temporal scales (Cai 2011, Bauer et al. 2013) requires more integrative C process and exchange measurements at the various terrestrial – aquatic – atmospheric interfaces over different time scales (tidal, diurnal and seasonal) to better understand the ecological functioning of these ecosystems facing global changes. Some studies in coastal wetlands such as salt marshes or tidal estuaries have taken water pCO_2 measurements at different temporal scales allowing the study of in situ CO_2 dynamics in relation to other biotic and abiotic processes. For instance, in Guanabara Bay (Brazil), water pCO_2 measured at high frequency, varying from 22 to 3715 ppmv, was negatively correlated with Chlorophyll *a* (Chl *a*) in surface waters, indicating that phytoplankton activity has an influence on CO_2 uptake and, more broadly, on inorganic C dynamics (Cotovicz Jr. et al. 2015). Moreover, Borges (2003) performed a 24-hour cycle in

June 2001 in an intertidal mangrove system (Gaderu Creek, India) and showed that water pCO_2 ranged from 1380 to 4770 ppmv with a strong control of these fluctuations by tides and biological activity (primary production and respiration). Within a small tidal creek of the Duplin River salt marsh-estuary coastal ecosystem (Georgia, USA), water pCO_2 calculated by Wang et al. (2018) showed strong seasonal and tidal/diurnal variations with winter values ranging from 500 to 4000 ppmv between high and low tide respectively, and summer values ranging from 1600 to 12000 ppmv between high and low tide respectively. However, still too few studies have taken high-frequency water pCO_2 measurements in salt marshes at the diurnal scale. These temporal variations in water pCO_2 strongly affect associated air-water CO_2 fluxes (FCO_2) that can, in turn, be estimated from the CO_2 gas transfer velocity, CO_2 solubility in the water and air-water CO_2 gradient (Borges 2003, Crosswell et al. 2017). The atmospheric Eddy Covariance (EC) technique represents an alternative way to directly measure in situ atmospheric CO_2 fluxes at the ecosystem scale (Baldocchi et al. 1988, Baldocchi 2003, Schäfer et al. 2014). This direct and non-intrusive micrometeorological method shows a growing interest in studying the metabolism of coastal ecosystems (sink or source) under real field conditions and to integrate them into regional C budgets (Polsenaere et al. 2012, Van Dam et al. 2021).

The purpose of this study is to better understand CO_2 dynamics at different temporal scales and locations over two aquatic sea – land continuums along the Atlantic French coast on Ré Island. These continuums include typical coastal systems (shelf, estuary, marsh) such as those studied elsewhere by Cai (2011) and Bauer et al. (2013) with regards to horizontal and vertical C exchanges in the coastal ocean. Unlike tidal salt marshes, which are more generally discussed in the literature, we studied two artificial salt marshes (i.e. salt ponds; Fig. A2) in which water exchanges are controlled by dykes and locks for human uses (biodiversity protection or anthropogenic activities). Through in situ high-frequency measurements of biogeochemical

parameters in waters and estimations of atmospheric CO_2 fluxes from 2018 to 2020, we sought to (1) describe water pCO_2 and associated CO_2 exchange variations at the diurnal, tidal and seasonal scales along the studied aquatic continuums, (2) identify biophysical drivers and the potential role of station typologies and salt marsh management practices on water pCO_2 and CO_2 budgets and (3) contextualize the associated continuum metabolism among other studied systems from a C dynamic and budget point of view.

2. Materials and methods

2.1. Study sites

2.1.1. Estuary (station *a*)

The Fier d'Ars represents a 750-ha maritime area within the French Atlantic Ocean (north of Ré Island), connected to the Breton Sound continental shelf by an opening that is 700 m wide (Fig. 1). It corresponds to a type II temperate tidal estuary according to Dürr et al.'s (2011) coastal system typology. With a maximum water height of 6.5 m, this tidal estuary exchanges between 2.4 and 10.2 million m^3 of coastal waters with the adjacent continental shelf depending on the tidal amplitudes (Bel Hassen 2001). At low tide (LT), its subtidal zone (in light blue; Fig. 1) is composed of mudflats (slikke) and tidal salt marshes (schorre) traversed by numerous channels converging toward a main channel measuring 300 m wide (Fig. 1). At high tide (HT), the subtidal zone is flooded by coastal waters up to the dykes (in red; Fig. 1), managed to control water exchanges between the estuary and artificial salt marsh complexes. These artificial salt marshes are old tidal salt marshes divided into multiple ponds mainly located along European coasts for which water residence times (from a few hours to fifteen days according to the management practices; Bel Hassen 2001) were originally controlled for

169 salt-farming (Tortajada et al. 2011). Nowadays, some of them are intended for other uses with
170 different water management practices based on their socio-economic activities (salt-, oyster-
171 and fish-farming or natural management; Fig. A2). The studied station *a* is located within this
172 tidal estuary, inside the subtidal zone of Fier d'Ars at its entry along the main channel connected
173 to the slikke (Fig. 1).

174

175 **2.1.2. Channel (station *b*)**

176 Station *b* is a secondary tidal channel associated to the schorre and located at the back
177 of the Fier d'Ars estuary just before the dyke (250 m wide at HT and 20 m wide at LT; Fig. 1).
178 With a maximum water height of 5.3 m at HT, it is connected to the tidal estuary station *a*
179 (distance of 1.6 km between stations *a* and *b*) enabling the supply of coastal water to artificial
180 salt marshes upstream from the dyke (Fig. 1).

181

182 **2.1.3. Rewilded artificial salt marsh (station *c*)**

183 For forty years, 121 ha of salt marshes within the Fier d'Ars system have been protected
184 and managed inside a National Natural Reserve (NNR) to encourage a high level of biodiversity
185 of migratory birds and vascular phanerogam and cryptogam developments (*Ruppia maritima*
186 and *Ruppia cirrhosa* in artificial salt marshes and *Zostera noltei* on mudflats; Champion et al.
187 2012). Within the terrestrial area of the NNR, artificial salt marshes communicate with Fier
188 d'Ars waters (station *a*) through lock management practices to promote biodiversity protection.
189 To the west, station *c* (surface area of 40100 m^2, depth of 60 cm) inside the NNR is a rewilded
190 artificial salt marsh supplied indirectly with coastal waters from the Fier d'Ars estuary by the

191 station *b* channel (distance of 500 m between stations *b* and *c*; Fig. 1) through a specific lock
192 management ensured by the NNR (former salt farm that has now been rewilded; Fig. A2). From
193 November until March (winter period), the marsh lock is open only at each full moon phase
194 when tidal amplitudes are higher than 70 in order to have the best compromise between salt-
195 and fresh-mixing waters (salinity around 30) to make it easier for aquatic fauna to pass from
196 the continental shelf to the marsh. On the contrary, from April to October when tidal amplitudes
197 are lower, the lock is permanently open to favour the development of *Ruppia sp.* seagrass beds
198 in the marsh with salinity varying between 30 and 46 (Champion et al. 2012). In past years, this
199 artificial salt marsh is also characterized by significant macroalgae development
200 (*Enteromorpha sp.* and *Ulva sp.*) at the subsurface and on sediments (Fig. A1) from early spring
201 to late summer each year thereby preventing seagrass development (Champion et al. 2012).

202

203 **2.1.4. Working artificial salt marsh (station *d*)**

204 To the east of the Fier d'Ars estuary, station *d* (surface area of 8500 m^2, depth of 75 cm)
205 also corresponds to an artificial salt marsh upstream from the dyke even though it directly
206 communicates (no channel in between) with the coastal waters of the Fier d'Ars estuary by a
207 dyke lock (distance of 2 km between stations *a* and *d*; Fig. 1). This second artificial salt marsh
208 was chosen for its specific lock management practice depending on the salt-farming activities
209 (working marsh) contrary to station *c* (rewilded marsh). In spring and summer, this working
210 marsh is particularly used for the storage of salt water in the context the salt-farming activity.
211 In this way, the lock is regularly open at this time of the year allowing upstream pond succession
212 supply to produce salt via evaporation between June and September (Fig. A2). Moreover, the
213 use of this artificial marsh for salt-farming activities requires a drying up and a cleaning once a

year in early spring before the start of the salt production period to remove seagrass, macroalgae and organic matter in the marsh (Poitevin, personal communication).

2.2.5. Other associated stations: continental shelf (station *Filiere W*) and tidal salt marsh (station *e*)

The Fier d'Ars estuary communicates with the Breton Sound which corresponds to a coastal maritime area on the French continental shelf between Ré Island and the continent (Fig. 1), characterized by a surface area of 425 km^2 and volume of 4920 million m^3 (Stanisiere et al. 2006, Soletchnik et al. 2014). The Breton Sound continental shelf exchanges large quantities of salt water with the Atlantic Ocean to the west at each semi-diurnal tidal cycle and it receives fresh water inputs through the Sèvre and Lay rivers within the Aiguillon Bay to the east (annual mean discharges of 44.4 and 14.0 m^3 s^{-1}, respectively) depending on hydrodynamic and meteorological conditions (Stanisiere et al. 2006, Soletchnik et al. 2014, Polsenaere et al. 2017). The highest and lowest river water flows were recorded in winter and summer, respectively, influencing the water salinity of the Breton Sound differently. Station *Filiere W* in the centre of the Breton Sound (Fig. 1) is located in a predominantly marine environment with a freshwater contribution of approximately 30 ml/l (i.e. 3%) from the Sèvre and Lay rivers (Stanisiere et al. 2006, Soletchnik et al. 2014). This additional station, studied by Coignot et al. (2020) using a different measurement strategy, was included in this study to contextualize the influence of the Breton Sound on our studied stations. At each HT, the Breton Sound supplies our studied coastal stations with various water masses based on the tidal amplitudes and seasonal periods along two aquatic sea – land continuums: (1) continental shelf (station *Filiere W*) – estuary (station *a*) – channel (station *b*) – rewilded artificial salt marsh (station *c*) and (2) continental

shelf (station *Filiere W*) – estuary (station *a*) – working artificial salt marsh (station *d*) (Fig. 1). Conversely, at each LT, different water masses from the artificial salt marshes are exported (indirectly through the station *b* channel for station *c* or directly for station *d*) to the Fier d'Ars estuary and then to the Breton Sound (Fig. A2).

Since June 2019, an atmospheric Eddy Covariance (EC) station (Campbell Scientific) has been deployed at station *e* (Fig. 1) to continuously measure in situ CO_2 fluxes at both the marsh-atmosphere and water-atmosphere interface at the ecosystem scale (Mayen et al. in prep). This tidal salt marsh station is located within the maritime NNR area with typical marsh vegetation (*Halimione sp.*, *Suaeda sp.* and *Spartina sp.*) emerged for 70% of time, during low tides and neap tides. In this study, only meteorological parameters (air temperature, rain, wind speed) corresponding to data from our four station measurement cycles were used from the EC station.

2.2. Measurement strategy and probes

In the subsurface water (~30 cm depth), partial pressures of CO_2 (pCO_2) and biogeochemical parameters (temperature, salinity, turbidity, dissolved oxygen and pH) were autonomously measured each minute with in situ probes deployed during fifteen 24-hour cycles at stations *a*, *b*, *c* and *d* during each season to record relevant temporal (diurnal, tidal and seasonal) and spatial (continuums) variations (Table A1). It should be noted that these seasonal measurement cycles were performed at one-day intervals (i) between stations *a* and *b* in 2018 and (ii) between stations *c* and *d* in 2019/2020 (Table A1). In situ measurements could not be taken at station *d* in spring 2020 due to the Covid pandemic. Over the Breton Sound continental shelf at station *Filiere W*, the same biogeochemical measurements were taken biweekly by Coignot et al. (2020) over the year 2018: four samplings in winter (17/01/2018 14:15;

30/01/2018 13:55; 15/02/2018 14:03; 03/03/2018 13:40), four samplings in spring (17/04/2018 14:25; 26/04/2018 12:20; 29/05/2018 13:40; 14/06/2018 14:00); four samplings in summer (28/06/2018 13:05; 11/07/2018 12:45; 09/08/2018 10:45; 11/09/2018 08:50) and five samplings in autumn (26/09/2018 13:45; 09/10/2018 13:25; 24/10/2018 12:50; 08/11/2018 08:15; 11/12/2018 09:50). At stations *b* and *c* in summer 2019, the water height, temperature and salinity were simultaneously measured every 10 min. by two STPS sensors (NKE Instrumentation) (unpublished results).

An autonomous pCO_2 underwater sensor (C-Sense^{TM} pCO_2 sensor, PME/Turner Designs), an EXO2 multiparameter probe (YSI) and a C3-submersible fluorimeter (Turner Designs) were deployed to measure water pCO_2, physicochemical parameters and fluorescence, respectively. Chlorophyll *a* concentrations were derived from the fluorescence data measured by the C3-fluorimeter every 10 min. as a proxy to study the dynamics of phytoplankton biomass over time (Aminot & Kérouel, 2004). This sensor was used only for summer 2019 and winter 2020. The measurement range of the C-Sense probe is 0-2000 ppmv with an absolute accuracy of 60 ppmv (3% of the full scale; Turner Designs). The EXO2 probe was used to measure the pH (NBS scale), temperature (in °C), salinity, dissolved oxygen concentration (DO in µmol l^{-1}), oxygen saturation percentage (O_2-sat. in %) and turbidity (in NTU). The maximum permissible errors of the different EXO2 sensors are 0.2 and 0.5 unit for pH and salinity respectively, 0.25 °C for temperature, 5 NTU for turbidity and 25 µmol l^{-1} for O_2 (YSI). Between each station, the EXO2 pH sensor was calibrated with three buffer solutions (pH 3, 7 and 10). It was not possible to measure pH values at stations *a* and *b* in 2018 (Table 2).

Water pCO_2 values measured by the C-Sense probe are influenced by the total dissolved gas pressure (TDGP) which corresponds to the total pressure exhibited by all gases within the

water column. When this pressure greatly exceeded the pressure at which the C-Sense was calibrated, the output needed to be corrected. Then, a pCO_2 correction was applied taking both TDGP and atmospheric pressure during sensor calibration (1009 hPa) and the measured pCO_2 by the C-Sense probe (gross values) into account, as per equation ($pCO_{2meas.}$ × 1009) / TDGP (Turner Designs). Over the fifteen 24-hour cycles performed at the seasonal and spatial scales, the corrected pCO_2 with TDGP were 2.6 ± 0.9% lower than the raw pCO_2 values.

2.3. Temperature and non-temperature effects on pCO_2 variations

To distinguish between the temperature and non-temperature effects on in situ pCO_2 variations at the seasonal and diurnal scales, $TpCO_2$ (pCO_2 variations related to temperature physical effects, in ppmv) and $NpCO_2$ (pCO_2 variations related to non-temperature effects, in ppmv) were calculated respectively, following (Eq. 1) and (Eq. 2) from Takahashi et al. (2002):

$$TpCO_2 = pCO_{2mean} \times \exp[0.0423 \times (T_{obs} - T_{mean})] \quad (1)$$

$$NpCO_2 = pCO_{2obs} \times \exp[0.0423 \times (T_{mean} - T_{obs})] \quad (2)$$

where T_{obs} and pCO_{2obs} are the temperature and pCO_2 values measured by the probes at each time step (1 min.), respectively. T_{mean} and pCO_{2mean} are the temperature and pCO_2 averaged either at the seasonal (annual mean) or diurnal scale (means per cycle). Whereas $TpCO_2$ is only associated with the physical pump, $NpCO_2$ is associated with biological processes, tidal advection and benthos-pelagos couplings that may be important in shallow coastal systems (Cotovicz Jr. et al. 2015, Polsenaere et al. 2022).

2.4. Calculations of air-water CO_2 fluxes

For all our measurement periods (Table A1), the gas transfer velocity (k_{600}) and hourly CO_2 fluxes (FCO_2) at the air-water interface were estimated following, for instance, Ribas-Ribas et al. (2011) and Polsenaere et al. (2022) in coastal environments. At stations *a* and *b*, only air-water FCO_2 during HT (four hours around each HT) were calculated, whereas at stations *c* and *d*, all hourly FCO_2 were calculated using the following formula (Eq. 3):

$$FCO_2 = \alpha \times k \times \Delta pCO_2 \quad (3)$$

where FCO_2 is the estimated CO_2 fluxes at the air-water interface (mmol m^{-2} h^{-1}), α is the CO_2 solubility coefficient in saltwater (mol kg^{-1} atm^{-1}), k is the gas transfer velocity of CO_2 (in cm h^{-1}) and ΔpCO_2 is the gradient between mean water and air pCO_2. Water pCO_2 (ppmv) were measured by the in situ C-Sense probe and atmospheric CO_2 concentrations (ppm) were measured by the EC station (station *e*; Fig. 1) during summer 2019 and winter 2020. For all other periods, atmospheric CO_2 data were obtained from the National Oceanic and Atmospheric Administration (NOAA) at the Mauna Loa Observatory in Hawaii (https://gml.noaa.gov/ccgg/trends/). The CO_2 solubility coefficient (α) depends on water temperature and salinity and was calculated according to Weiss (1974). The gas transfer velocity (*k*) also significantly controls air-water FCO_2 since it directly takes turbulence processes at the air-water exchange interface into account (Polsenaere et al. 2013). In this study, k (or k_{660}) was calculated according to both Raymond & Cole (2001) (RC01; Eq. 4) and Wanninkhof (1992) (W92; Eq. 5) corresponding to closed environments and more open coastal environments, respectively. These two parametrization methods for the k exchange coefficient were applied to the four stations in order to compare the results.

For closed freshwater environments (Raymond & Cole 2001),

$k_{600} = 1.91 \times \exp[0.35 \times U10]$ (4)

For more open coastal environments (Wanninkhof 1992),

$k_{600} = 0.31 \times (U_{10})^2$ (5)

The gas transfer coefficients normalized to a Schmidt number of 600 (k_{600}) obtained with the two parametrization were then converted to the gas transfer velocity of CO_2 at the in situ temperature and salinity (k_{660}) according to Jähne et al. (1987) as per the equation (6):

$k_{660} = k_{600} / (660/Sc)^{-0.5}$ (6)

where k_{660} is the gas transfer velocity of CO_2 at the in situ temperature and salinity (cm h^{-1}) according to the parametrizations of RC01 or W92, U_{10} is the wind speed normalized to 10 m (m s^{-1}) using the relationship of Amorocho & DeVries (1980) and Sc is the Schmidt number which describes both the water viscosity and the molecular diffusion of the subsurface layer (Bade 2009). In summer 2019 and winter 2020, wind speed data were measured by the EC station at a height of 3.15 m (station *e*; Fig. 1); for all other periods, wind data were obtained from the "Infoclimat" station on Ré Island (Fig. 1) measured at a height of 10 m (6.20, 4.85, 4.30 and 8.40 km from stations *a*, *b*, *c* and *d* respectively).

2.5. In situ Chl *a* concentrations and fluorimeter data calibration

In situ Chl *a* concentrations were measured from samples collected at stations *c* and *d* following Aminot & Kérouel (2004). Water samples (50 ml) were filtrated (47 mm Whatman GF/F filter) and Chl *a* filters were kept at -18°C up to analysis. In the laboratory, in the dark, pigments were extracted in a 90% acetone solvent at the same time the filter was crushed with a glass rod. After one night of stirring at 4 °C to continue the extraction and a 10-min

centrifugation at 3000 rpm, the supernatant absorbance was measured by spectrophotometry at 665 nm to obtain the Chl *a* level (its absorbance peak is at 665 nm). Chl *a* were measured from eight water samples except at station *c* in spring. Chl *a* could not be measured at stations *a* and *b* in 2018.

For the fluorimeter data, the calibration procedure was applied to derive Chl *a* concentrations from our 10 min-water fluorescence measurements. Chl *a* concentrations were calculated through the significant ($p < 0.05$) linear regressions obtained for each deployment (summer 2019 and winter 2020) between C3-submersible fluorimeter data and the in situ Chl *a* concentration analysis from sub-surface waters (eight samplings on average per each 24 hour-cycle) sampled simultaneously right at the fluorescence probe.

2.6. Statistical tools and analysis

For all measured variables, the data did not respect a normal distribution (Shapiro-Wilk, $p < 0.05$). Shapiro-Wilk tests and non-parametric comparison tests such as the Mann-Whitney and Kruskal-Wallis tests were carried out with 0.05 level of significance. A Dunn test was used to perform a post-hoc multiple comparison of the Kruskal-Wallis test to detect significant differences among groups. The R-studio software was used to perform the principal component analysis ("FactoMineR" package; Lê et al. 2008) and the Spearman correlation matrices ("corrplot" package; Wei and Simko 2017). A PCA was carried out to study the contribution of the variables to the data at the spatial and seasonal scales. It is based on the mean values of the physicochemical and biogeochemical parameters of water (temperature, salinity, turbidity, dissolved oxygen, oxygen saturation and water pCO_2) for each 24-hour cycle at stations *a*, *b*, *c*

and *d*. Temporal graphs, linear regressions, boxplots and barplot were performed with the GraphPad Prism 7 software.

Total alkalinity (TA) were estimated at the diurnal scale from the measured salinity, temperature, pH and water pCO_2 using the carbonic acid constant from Mehrbach et al. (1973) as modified by Dickson and Millero (1987), the K_{HSO4} constant from Dickson (1990) and the borate acidity constant from Lee et al. (2010).The CO_2 system calculation programme (version 2.1.) was used to perform these calculations (Lewis and Wallace, 1998).

3. Results

3.1. Biogeochemical overview of the shelf – estuary – marsh water continuums

Over our measurement periods, meteorological conditions for the years 2018 and 2019 were similar with regard to air temperatures. The thermal conditions followed a classical seasonal trend with the highest and lowest temperatures measured in summer (July 2018 and 2019) and in winter (March 2018 and February 2020), respectively (Table 1). However, the months of July 2018, July 2019 and February 2020 were warmer (+2.1, +2.4 and +3.2 °C, respectively) than the reference period (1981-2010). Annual cumulative precipitations were lower in 2018 than in 2019 (786 and 827 mm, respectively); March 2018 and October 2019 were the rainiest months (+82 and +41%, respectively, compared with the 1981-2010 period; Table 1). Salinity values measured by the French Phytoplankton Monitoring Network REPHY at station *Filiere W* as the water source flowing into the two aquatic continuums did not vary significantly between the years 2018, 2019, 2020 and the 2000-2017 period (Kruskal-Wallis test, $p = 0.77$; Fig. A3).

At the station *Filiere W* continental shelf, the highest and lowest Chl *a* concentrations were recorded in winter (2.0 ± 0.0 µg l^{-1}) and in summer (3.0 ± 1.2 µg l^{-1}), respectively (Coignot et al. 2020). In the artifical salt marshes, in summer 2019, autumn 2019 and winter 2020 (Table A1), the Chl *a* concentration varied significantly at the spatial scale (Mann-Whitney tests, $p < 0.05$). For example, at stations *c* and *d*, in situ Chl *a* averaged 5.4 ± 1.6 and 1.9 ± 0.3 µg l^{-1}, respectively in summer 2019, and 1.3 ± 0.3 and 3.4 ± 0.4 µg l^{-1}, respectively in winter 2020. At station *c* during spring 2019, an important macroalgae development (*Enteromorpha sp.* and *Ulva sp.*) was observed in the subsurface waters and on sediments in the marsh up to autumn (Fig. A1). On the contrary, at station *d* in 2019 and 2020, no macroalgae development occurred, allowing for the growth of *Ruppia sp*. seagrasses in the marsh (Fig. A1).

At station *Filiere W* in 2018, over the biweekly measurement periods, water temperature values varied from 7.5 (winter) to 21.7 °C (summer) whereas at station *a* over our seasonal 24-hour cycles (high-frequency measurements), values varied from 9.1 (winter) to 26.9 °C (summer). Along the studied aquatic continuums, the water temperature varied significantly between stations *a* and *b* (Mann-Whitney test, $p < 0.05$) and between stations *a* and *c* ($p < 0.05$) but no significant variation was recorded between stations *b* and *c* ($p = 0.23$) (Table 2). Salinity ranged from 28.9 (winter) to 35.4 (autumn) at station *Filiere W*, whereas values varied from 31.4 (winter) to 35.7 (autumn) at station *a*, from 27.5 (winter) to 36.9 (autumn) at station *b*, from 27.0 (winter) to 42.6 (summer) at station *c* and from 21.3 (winter) to 38.4 (autumn) at station *d* with higher salinity gradients at stations *c* and *d* (artificial salt marshes) than at stations *a* and *b* (tidal estuary and channel). In average over the year 2018, the tidal estuary (station *a*) was slightly oversaturated in oxygen compared to the atmosphere (106 ± 14%) with O_2-sat. values ranging between 70% (LT during dawn) and 147% (receving tide the day) during the summer cycle (Fig. 3). Along the continuum, the channel (station *b*) was close to the

saturaturion value with the atmosphere over the same measurement periods in 2018 with a lower maximum value (120%) than at station *a* measured in summer (Fig. 4). Larger amplitudes of oxygen saturation percentages were recorded in the artificial salt marshes with O_2-sat. values ranging from 36 to 176% at station *c* (over the summer cycle; Fig. 5) and from 49 to 150% at station *d* (over the summer cycle; Fig. 6). The annual percentage of pCO_2 undersaturation compared to the atmosphere were 47.8%, 15.9%, 64.9% and 85.9% at stations *a*, *b*, *c* and *d* respectively, with a strong annual CO_2 oversaturation at station *b* (Table 2). Moreover, along aquatic continuums, the greatest amplitude in water pCO_2 was recorded at station *c* with values varying between 6 ppmv in spring 2019 (macroalgae bloom and undersaturated in CO_2) and 721 ppmv in autumn 2019 (macroalgae degradation and oversaturated in CO_2).

3.2. Spatial and seasonal dynamics of studied continuum waters

Significant spatial variations in water pCO_2 and associated biogeochemical parameters (salinity, temperature, turbidity and DO) were recorded along shelf – estuary – marsh water continuums (Kruskall-Wallis tests, $p < 0.05$; Table 2). The PCA reveals that stations are distinguished vertically according to pCO_2, turbidity and oxygen saturation (pCO_2 and O_2-sat. negatively correlated) within PC2 explaining 35.5% of the total variance (Fig. 2). We can cleary observe that the water pCO_2 values measured biweekly at station *Filiere W* were higher than the station *a* values measured over our 24-hour cycles (Fig. 2). On average over the year, the station *b* channel had the highest pCO_2 values (462 ± 51 ppmv) compared to the three other stations studied (418 ± 57, 335 ± 214 and 293 ± 113 ppmv, respectively at stations *a*, *c* and *d*; Fig. 2). Station *b* was also characterized by the highest water turbidity with values ranging from 1.6 to 59.7 NTU (median of 8.2 NTU) whereas at station *a*, the values only varied from 0.1 to

32.6 NTU (median of 1.9 NTU). The PCA also shows seasonal data are distinguished horizontally according to salinity and temperature within PC1 explaining 42.3% of the total variance (Fig. 2). Generally, for each station, the highest and lowest temperature and salinity values were measured in summer and winter, respectively (Fig. 2) except at station *a* where the lowest salinity values were recorded in spring (Table 2). Within each station, significant differences in the temperature and salinity values were recorded at the seasonal scale (Kruskall-Wallis tests, $p < 0.0001$).

Along the continuums, the PCA recorded contrasted seasonal variations of water pCO_2, particularly between the two artifical salt marshes (Fig. 2). At the station *Filiere W* continental shelf in 2018, no significant differences in water pCO_2 were recorded at the seasonal scale (Kruskall-Wallis test, $p = 0.13$), although the highest and lowest seasonal means were recorded in winter and spring, respectively (Table 2). At the station *a* estuary in 2018, water pCO_2 showed the same seasonal pattern decreasing from winter (441 ± 21 ppmv) to spring-summer (390 ± 40 and 385 ± 60 ppmv, respectively) before increasing in autumn (460 ± 58 ppmv), whereas the station *b* channel showed lower seasonal variations over the same measurement periods (Table 2 and Fig. 2). In contrast to the tidal stations (*Filiere, a* and *b*), artificial salt marshes (*c* and *d*) showed larger seasonal pCO_2 variations (Fig. 2). Station *c* waters were undersaturated in CO_2 with respect to the atmosphere both in spring 2019 (135 ± 165 ppmv), summer 2019 (242 ± 116 ppmv) and winter 2020 (343 ± 87 ppmv) but oversaturated in autumn 2019 (622 ± 57 ppmv). At the same time and on average, station *d* was undersaturated in CO_2 in summer, autumn and winter with the largest water CO_2 undersaturation recorded in autumn (155 ± 30 ppmv) in contrast to station *c*. At each studied station (*a*, *b*, *c* and *d*), water pCO_2 significantly differed at the seasonal scale (Kruskall-Wallis tests, $p < 0.001$), except for station *a* between spring and summer (Dunn's post-test, $p > 0.999$).

At stations *a* and *b* in 2018, the same seasonal $NpCO_2$ variations were observed, decreasing from winter (595 and 624 ppmv, respectively) to summer (296 and 347 ppmv, respectively) and then increasing towards autumn (420 and 439 ppmv, respectively). At station *c*, the seasonal mean $NpCO_2$ value increased sharply from summer 2019 (193 ppmv) to autumn 2019 (630 ppmv) and then decreased towards winter 2020 (441 ppmv), contrarily to station *d* where, values decreased from summer (286 ppmv) to autumn 2019 (160 ppmv) before increasing towards winter 2020 (453 ppmv) to reach a similar seasonal $NpCO_2$ value as station *c*. Regarding temperature effects on water pCO_2, the lowest and highest seasonal $TpCO_2$ values were measured in winter and summer, respectively, with seasonal $TpCO_2$ values followed systematically seasonal water temperature variations. At stations *a* and *b*, weak seasonal pCO_2 variations were recorded with the $TpCO_2$ effects offset by the $NpCO_2$ effects, particularly in winter and summer. Conversely, in artificial salt marshes, the water $NpCO_2$ and pCO_2 values followed the same seasonal patterns in spring, summer and autumn at station *c* and only in autumn at station *d* (Fig. A4).

3.3. Biogeochemical variations at diurnal and tidal scales

Over all 24-hour measurement cycles, the measured parameters showed strong variations at the diurnal/tidal scales (Figs. 3-6). At station *a* in winter, only small tidal salinity variations were measured (31.9 - 32.9; Fig. 3), whereas at station *b* over the same measurement period, the largest tidal salinity variations occurred with values varying from 27.5 at LT to 32.5 at HT (Fig. 4). On the contrary, at stations *a* and *b* during summer and autumn, lower salinity gradients were measured and salinity values were higher at LT than at HT (Figs. 3 and 4). In the two artificial salt marshes, the highest salinity gradients were recorded in summer with

487 values decreasing through coastal water inflows from 42.6 to 33.5 at station *c* (Fig. 5) and from
488 38.1 to 33.8 at station *d* (Fig. 6). During the other seasons at the diurnal/tidal scales, salinity
489 values varied more slightly with, for instance, a difference in salinity units of 2.7, 0.7 and 1.1
490 at station *c* in winter, spring and autumn, respectively (Fig. 5). It should be noted that, at station
491 *c*, coastal water inflows from station *b* led to an increase in salinity only in winter (Fig. 5); in
492 autumn, a rainfall event occurred (5 mm) between 14:00 and 15:00 leading to a decrease in
493 salinity of 1 unit, an increase in turbidity from 2.7 to 7.3 NTU (peak at 15.7 NTU) but without
494 any water pCO_2 variation (Fig. 5). At station *d*, turbidity and salinity did not vary both in autumn
495 and winter cycles (Fig. 6).

496 The largest diurnal/tidal variations in the water pCO_2 and DO concentrations occurred
497 during summer with pCO_2 gradients of 255, 216, 405 and 258 ppmv at stations *a*, *b*, *c* and *d*
498 respectively, and DO gradients of 153.2, 152.2, 262.8 and 205.6 µmol l^{-1} at stations *a*, *b*, *c* and
499 *d*, respectively (Figs. 3-6). At stations *a* and *b*, the low tide periods during the day (LT/D)
500 occurring at dawn showed higher water pCO_2 and lower O_2-sat. values than the low tide periods
501 during the night (LT/N) occurring at dusk, particularly in summer (Figs. 3 and 4). In general,
502 our diurnal cycles showed a decrease in pCO_2 that was negatively correlated to an increase in
503 DO during the daytime (except at station *c* in spring; Fig. 5) and an opposite pattern during the
504 night-time (except at station *c* in summer; Fig. 5). For instance, at station *c* in winter during the
505 marsh confinement, water pCO_2 decreased from 519 to 129 ppmv during the day (from 09:00
506 to 17:00) and increased from 212 to 442 ppmv during the night (from 20:00 to 05:00), while
507 DO increased from 273.4 to 350.0 µmol l^{-1} and decreased from 286.5 to 257.5 µmol l^{-1},
508 respectively (Fig. 5). It should be noted that, at station *c* in summer, the lowest DO
509 concentration and O_2-sat. percentage were reached during the night (76.9 µmol l^{-1} and 35.6%,
510 respectively; Fig. 5). At station *d*, the same diurnal water pCO_2 and DO patterns were also

observed (Fig. 6). However, these measured diurnal pCO_2 and DO variations were significantly disrupted once coastal water horizontal advection and artificial salt marsh management practices occurred (Figs. 3-6).

Strong tidal variations in water pCO_2 were generally recorded during all seasons except at station *d* both in autumn and winter (Fig. 6). At stations *a* and *b*, incoming tides during the day produced rapid decreases in water pCO_2 from an oversaturation to a slight undersaturation of subsurface waters compared to the atmosphere, particularly in spring (-121 and -167 ppmv, respectively) and summer (-139 and -115 ppmv, respectively; Figs. 3 and 4). Only at station *a*, receding tides during the day generated an additional decrease in pCO_2 to reach the lowest values measured within each season (270 and 335 ppmv in summer and autumn, respectively; Fig. 3). Then, at station *a* in winter and spring, incoming tides during the night produced slight increases in water pCO_2 whereas in summer and autumn at the same station and at station *b* over the four seasons, incoming tides during the night-time produced strong increases in pCO_2 leading to oversaturation periods (Figs. 3 and 4). Through simultaneous salinity measurements at stations *b* and *c* and a cross-correlation function analysis, we estimated the horizontal advection of water masses from station *b* to station *c* during a spring tide period at 90 minutes (periods from 29/06 to 08/07/2019). At station *c* during the night, higher pCO_2 were measured at HT than at LT (i) in spring (363 ± 85 and 16 ± 5 ppmv at HT/N and LT/N, respectively), (ii) in summer (295 ± 46 and 258 ± 37 ppmv at HT/N and LT/N, respectively) and (iii) in winter (431 ± 6 and 323 ± 53 ppmv at HT/N and LT/N, respectively; Fig. 7). The same tidal pCO_2 pattern was also recorded at this station in summer 2019 during the day (323 ± 88 and 197 ± 141 ppmv at HT/D and LT/D, respectively; Fig. 7). In spring, the rewilded artificial marsh (station *c*) recorded very low water pCO_2 values both the day and the night during the marsh

534 confinement but coastal water inflows from the station *b* channel instantly produced a large and
535 rapid increase in water pCO_2 (+390 ppmv) mostly within a two-hour period (Fig. 5).

536 For all 24-hour cycles, there were strong positive correlations between pCO_2 and $NpCO_2$
537 showing that non-temperature effects have a strong control over water pCO_2 at the diurnal/tidal
538 scale along the two studied continuums (Figs. 3-6). Similarly, water pCO_2 values were strongly
539 negatively correlated with oxygen saturation, especially in autumn with diurnal correlations
540 between pCO_2 and O_2-sat. ranging from -0.67 (winter) to -0.97 (autumn) at station *a*, from -
541 0.63 (summer) to -0.87 (autumn) at station *b*, from -0.54 (winter) to -0.86 (autumn) at station *c*
542 and from -0.59 (winter) to -0.84 (summer) at station *d* (Figs. 3-6). At the artificial salt marsh
543 stations, correlations between pCO_2 and in situ Chl *a* were -0.62 and -0.47, respectively in
544 winter and summer at station *d* (Fig. 6) and -0.41 in winter at station *c* (Fig. 5). At station *c* in
545 summer, correlations between pCO_2 *vs.* DO and pCO_2 *vs.* Chl *a* were not significant but the
546 pCO_2 *vs.* salinity coefficient was -0.95 (Fig. 5). At station *b*, significant linear regressions were
547 calculated between pCO_2 and salinity, i.e. negative in spring ($R^2 = 0.49$) and positive in summer
548 ($R^2 = 0.53$; Fig. 7). Lastly, at station *c*, a negative pCO_2 *vs.* salinity regression was also
549 calculated both in spring and summer ($R^2 = 0.83$ and $R^2 = 0.87$, respectively) with a positive
550 water pCO_2 *vs.* water height correlation ($R^2 = 0.72$) observed at station *c* in summer (Fig. 7).

551

552 **3.4. Air-water CO_2 flux variations and associated salt marsh metabolism**

553 Mean air-water CO_2 fluxes (FCO_2) according to the W92 parametrization were
554 estimated to be -0.01 ± 0.22, 0.22 ± 0.40, 0.18 ± 1.37 and -1.22 ± 1.71 mmol m^{-2} h^{-1} at stations
555 *a* (sink), *b* (source), *c* (source) and *d* (sink), respectively, whereas the downstream point of each
556 studied continuum (station *Filiere W*) behaved as a net CO_2 source (0.30 ± 1.04 mmol m^{-2} h^{-1}).

Large seasonal variations were observed at the four studied stations (Fig. 8). On average, station *a* showed positive FCO_2 values in both winter and autumn (slight CO_2 source) but negative means in spring and summer (slight CO_2 sink; Table 3 and Fig. 8). At the station *b* channel, positive FCO_2 values were estimated, with maximun and minium FCO_2 mean values occurring in winter (0.52 ± 0.65 mmol m^{-2} h^{-1}) and summer (0.06 ± 0.08 mmol m^{-2} h^{-1}), respectively (Fig. 8). Station *c* behaved as a CO_2 sink in spring, summer and winter whereas it emitted large quantities of CO_2 to the atmosphere in autumn (2.03 ± 1.17 mmol m^{-2} h^{-1}; Fig. 8). FCO_2 values at station *c* varied between -3.00 and 0.03 mmol m^{-2} h^{-1} in spring and between 0.61 and 4.61 mmol m^{-2} h^{-1} in autumn. Lastly, station *d* behaved as a CO_2 sink in summer, autumn and winter with the largest atmospheric CO_2 uptake in autumn (-3.43 ± 1.09 mmol m^{-2} h^{-1}) where fluxes varied between -6.03 and -1.79 mmol m^{-2} h^{-1} (Fig. 8). At the global scale (stations *a*, *b*, *c* and *d*), the Fier d'Ars system behaved as a CO_2 sink over the year (-0.20 ± 1.32 mmol m^{-2} h^{-1}) with (i) the lowest FCO_2 values recorded during the growing season in spring and (ii) higher FCO_2 values during the night than during the day.

4. Discussion and conclusions

4.1. Water pCO_2 dynamics according to the typologies of the shelf – estuary – marsh continuums

Along the studied continuum stations from the coastal ocean to artificial salt marshes, significant water pCO_2 variations were recorded at the spatial scale (Fig. 9). A strong influence of ecosystem typology (continental shelf, estuary, marsh) on inorganic C dynamics was observed, as described more generally by Bauer et al. (2013) for the coastal ocean. In 2018 and 2019, the continental shelf (station *Filiere W*), influenced by the Aiguillon Bay and its

associated watershed, was characterized by salinity ranges below those from the Atlantic Ocean (35.6; Vandermeirsch 2012). This was confirmed by the French Phytoplankton Monitoring Network REPHY for the 2000-2017 period with values between 26.2 and 35.8 (Fig. A3; Belin et al. 2021). At station *Filiere W*, the lowest salinity values were measured in winter when terrestrial river inputs from the Aiguillon Bay watershed were the highest leading to strong nutrient inputs into coastal waters during this time period (Belin et al. 2021). However, in 2018, the non-significant relationship found between salinity and pCO_2 ($p = 0.88$) measured biweekly at station *Filiere W* showed a rather weak influence of terrestrial inputs on pCO_2 dynamics. At this shelf station, phytoplankton blooms generally occur in spring and summer (Coignot et al. 2020), inducing an undersaturation of water CO_2, followed by pCO_2 decreases observed at station *a* along the continuum. Station *a*, found at the entry of the Fier d'Ars estuary, is influenced by buffered marine waters from the shelf with the percentage of CO_2 oversaturation over a 24-hour cycle varying from 96% (winter) to 18% (spring/summer). This decrease in water pCO_2 could be attributed to phytoplankton development in the estuarine waters during this period. The fact that the seasonal $NpCO_2$ (non-temperature effects on pCO_2) varied from heterotrophy in winter to autotrophy in summer confirmed the phytoplankton activity on the pCO_2 dynamics. Another study carried out close to station *a* measured Chl *a* concentrations between 0.2 (winter) and 3.5 µg l^{-1} (spring/summer) and a net Chl *a* export suggestive of a net primary production within this tidal estuary (Bel Hassen 2001). Moreover, microphytobenthos (MBP) may also contribute to water CO_2 undersaturation at station *a* and to the overall water column Chl *a* concentration through tidal resuspensions as shown by Savelli et al. (2019) in a nearby intertidal zone. Due to the small insulary catchement area (1200 ha) consisting only of salt marshes (no terrestrial water input), the CO_2 dynamics in the Fier d'Ars estuary (station *a*) is different from other estuaries worldwide (Borges & Abril 2011). Low water pCO_2 values

(270 - 569 ppmv) with no significant relationship between pCO_2 and salinity were found, like in the present study and elsewhere on the Atlantic coast of the United States (Jiang et al. 2008), thereby enabling potential CO_2 sink behaviours (Maher & Eyre 2012). Similarly, the marine-dominated estuary of Sapelo Sound (USA) was also characterized by lower water pCO_2 values than river-dominated estuaries (Borges & Abril 2011). However, the water pCO_2 values measured at this estuary (390 - 2400 ppmv) were higher than those measured at station *a* in our study due to high bacterial mineralization rates of organic carbon (OC) produced by *Spartina* in nearby tidal salt marshes (Jiang et al. 2008). On the contrary, river-dominated estuaries characterized by strong freshwater inputs generally show much higher pCO_2 values. The heterotrophic status due to the microbial degradation of OC from rivers produces large CO_2 degassing into the atmosphere (Borges & Abril 2011, Bauer et al. 2013, Najjar et al. 2018) as observed nearby in the Aiguillon Bay (Coignot et al. 2020), the Gironde estuary (Frankignoulle et al. 1998) and the Loire estuary (Abril et al. 2009).

Overall, the studied channel (station *b*) between the tidal estuary and artificial salt marshes (Fig. 9) showed longer periods of CO_2 oversaturation over the year 2018 (90, 73 and 100% in winter, spring/summer and autumn, respectively) with significantly higher water pCO_2 values than those at the station *a* estuary. At station *b*, strong hydrodynamic forcings during incoming and receding tides produced more turbid waters due to organic matter (OM) resuspension from channel muds (Fig. 4). Then, it probably limited the activity of primary producers (phytoplankton, algae, plants) and, on the contrary, favoured heterotrophic processes (Polsenaere et al. 2022). In the Fier d'Ars waters close to station *b*, Tortajada (2011) measured POC/Chl *a* > 200 on average over the year and POC/Chl *a* > 600 in autumn. This may confirm a microbial loop-type trophic network in channel waters (Tortajada 2011) and a potential influence on the C dynamics leading to OM mineralization processes from MPB and, in turn,

water CO_2 oversaturation periods measured at station *b*. However, channel waters showed lower pCO_2 values compared with other coastal channel systems probably due to very low terrestrial water inputs upstream/downstream over the Fier d'Ars estuary. In the Arcachon lagoon, Polsenaere et al. (2022) recorded at a tidal channel similar to stations *a* and *b* according to typology, long periods of CO_2 oversaturation with seasonal means ranging from 461 ± 14 in July 2008 to 530 ± 39 ppmv in September 2009. Another study showed that the Sancti Petri Channel waters and the adjacent salt marsh system linking the Atlantic Ocean to the Cadiz Bay were mainly CO_2 oversaturated similarly to our station *b*, with an annual pCO_2 mean of 564 ± 134 ppmv (281 - 862 ppmv), due to OM diagenetic processes in mudflats that could constitute a DIC source in the water column and thus increased water pCO_2 (Burgos et al. 2018). Within the Duplin River salt marsh-estuary coastal system, higher summer pCO_2 values and DIC concentrations were recorded at low tide in channel waters (12000 ppmv and 4300 µmol l^{-1}, respectively) than at high tide in marsh waters (1600 ppmv and 2200 µmol l^{-1}, respectively; Wang et al. 2018).

Contrary to tidal stations (*a* and *b*), significant and more pronounced periods of CO_2 undersaturation were recorded in artificial salt marsh waters (76 and 87% at stations *c* and *d*, respectively), once again indicating that marsh typology has a strong influence on CO_2 dynamics. In shallow coastal wetlands such as artificial salt marshes, lower hydrodynamic conditions and longer water residence times promote the development of primary producers such as macrophytes and phytoplankton and as a result, biological CO_2 uptake (Wang & Cai 2004, Bauer et al. 2013, Tobias & Neubauer 2019). The artificial salt marsh waters studied here showed lower pCO_2 values and longer CO_2 undersaturation periods, particularly in spring and summer due to strong macrophyte activity (i.e. macroalgae at station *c* and seagrasses at station *d*) compared with other marshes and wetland types (Cotovicz Jr. et al. 2015, Wang et al. 2018,

652 Berg et al. 2019). By comparison, Ternon et al. (2018) measured higher water pCO_2 in nearby
653 fresh- and brackish-water artificial marshes on the French Atlantic coast in summer 2018 with
654 values varying between 227 and 1925 ppmv and between 349 and 2000 ppmv, respectively.
655 Unlike seagrass beds (Mcleod et al. 2011), fast-growing macroalgae developing in coastal
656 wetlands such as at station *c* have a limited capacity to store C over the long-term. However,
657 other studies have shown their potential contribution to coastal blue C by (i) storing large OM
658 quantities in their living biomass through their high primary production (Raven 2018) and (ii)
659 transferring it to adjacent systems through tides and storage in coastal sediments (Duarte &
660 Cebrián 1996, Hill et al. 2015, Krause-Jensen & Duarte 2016).

661

662 **4.2. Marsh management practices module temporal carbon dynamics**

663 Management practices at the studied artificial salt marshes (stations *c* and *d*) correspond to
664 specific water lock management approaches linked to economic activities. They can strongly
665 modulate coastal water fluxes from the Fier d'Ars estuary (station *a*) and thereby influence
666 salinity and marsh pCO_2 dynamics. At station *c* in 2019, the specific management practice
667 undertaken by the NNR (see M&M section), along with higher air temperatures and lower
668 precipitations in summer, produced favourable conditions for macroalgae development from
669 early spring to late summer favoured by low marsh hydrodynamics and large temperature
670 fluctuations (Newton & Thornber 2013). To explain the observed macroalgae bloom, we also
671 assumed there were excess nutrient inputs, as described for other coastal ecosystems (Teichberg
672 et al. 2010). Nearby marsh aquafarming activities occurring upstream from the Ré Island
673 watershed that can communicate through the station *b* channel to station *c* may result in high
674 nutrient intake and could explain the macroalgae development (Paticat 2007, Tortajada 2011).

675 At station *b* in September 2018, DIN > 55 µmol l^{-1} and DIP > 5 µmol l^{-1} were measured at
676 ebbing tide (unpublished results). Moreover, shelf waters influenced by terrestrial inputs (see
677 the above paragraphs in the Discussion) could also lead to high nutrient inputs at marsh station
678 *c* through incoming tides. At station *Filiere W*, NO_3^- values ranged between 29 and 107 µmol
679 l^{-1} in winter 2019 and between 0.9 and 17.4 µmol l^{-1} in spring 2019 (Belin et al. 2021).
680 Consequently, at station *c* from spring, macroalgae communities probably prevented the
681 development of phytoplankton and seagrasses by marsh nutrient depletion and by light
682 limitation in the water column (Gouazé 2019). However, these fast-growing macrophytes
683 induce intense CO_2 uptake as observed in spring and summer 2019 (Fig. 5). During this period,
684 strong $NpCO_2$ effects confirmed the major influence of macroalgae biological autotrophy on
685 inorganic C dynamics (Fig. A4); large CO_2 undersaturation periods over tidal/diurnal cycles
686 were maintained although modulated by occasional coastal water inflows under weak tidal
687 amplitudes from station *b* into the marsh (Fig. 5). This result is confirmed by higher salinity
688 values at station *c* than at station *b* measured in spring and summer during our sampling periods
689 (Table 2). Other strong CO_2 undersaturation periods were recorded at station *c* in summer 2019
690 with a water pCO_2 mean of 297 ± 150 ppmv over a 96-hour cycle in early August ($2 < pCO_2 <$
691 723 ppmv; unpublished results). Therefore, these marsh waters were characterized by very low
692 pCO_2 values rarely observed over other similar wetland typologies (Borges 2003, Wang et al.
693 2018, Burgos et al. 2018, Berg et al. 2019). On the contrary, in autumn 2019, macroalgae
694 degradation probably by microbial mineralization processes produced the highest pCO_2 values
695 and largest water oversaturation periods recorded in the marsh waters. This result can be
696 explained by high NH_4^+ concentrations recorded in November 2019 (62 µmol l^{-1}; unpublished
697 results) and the lowest oxygen saturation values (Table 2).

Contrarily to station *c*, the working artificial marsh (station *d*) is managed for salt production in the upstream ponds along the continuum (Fig. A2) and is directly connected to the Fier d'Ars estuary (station *a*) with no channel connecting the two (Fig. 9). Salt production requires a subtle lock hydraulic management of the salt marsh depending on the frequency of the coastal water supplies that are mainly controlled by the salt manufacturer and meteorological conditions (rainfall, sunshine and wind) for evaporation (Paticat 2007). Therefore, contrary to station *c*, coastal water inflows to station *d* were generally performed sparingly with relatively small daily volumes to limit these water mixing effects (i.e. rapid accumulation of large water volumes through rainfall events or spring tides that stop the increase in temperature and salinity of the water already present in the marsh; Paticat 2007). At station *d* in summer 2019, the measured water pCO_2 values were significantly higher than those at the same period at station *c* but were very similar to those from station *a* in summer 2018 (Table 2). This result could be attributed to low activity of the primary producers during this period dedicated to salt production and confirmed by the significant thermal effects on water pCO_2 observed at this station unlike at station *c* (Fig. A4). A higher frequency of repetitive and direct water inflows through a specific lock management approach from station *a* to station *d* (similar mean summer salinity values at stations *a* and *d*; Table 2) could also explain these higher pCO_2 values. In autumn 2019 and winter 2020, lower hydrodynamic conditions due to lock closure (the salt farming activity was at a standstill; see M&M section) may have led to lower water turbidity values, lower nutrient inputs from shelf waters and then growth of *Ruppia sp.* seagrasses and phytoplankton in the marsh instead of macroalgae, thereby producing very low pCO_2 values.

Anthropogenic management practices in artificial salt marshes can therefore strongly influence the contribution and turnover of macrophytes and, consequently, the marsh CO_2 behaviour (sink/source). Due to eutrophication in the rewilded marsh (station *c*), development

of the macroalgae communities favoured an atmospheric CO_2 sink during the growing season but an overall annual net atmospheric CO_2 source through their degradation. Their presence prevents phytoplankton blooms and the establishment of seagrass beds as well as economic activities requiring specific management practices. Our work suggests a confinement of artificial marshes in winter and a drying up like at station *d* to avoid the nutrient inputs and the macroalgae development favouring rather slow-growing macrophytes such as seagrasses which could ultimately contribute to blue C sequestration as more generally described by Mcleod et al. (2011). Similarly, other studies have suggested that the coastal ecosystem management by reducing anthropogenic nutrients could favour blue C ecosystems such as seagrasses, salt marshes and C sequestration (Macreadie et al. 2017, Palacios et al. 2021). Few studies on the links existing between the functioning and C biogeochemical processes of artificial salt marshes have been carried out as in our study. For instance, in Mediterranean poly-euhaline lagoon waters, Le Fur et al. (2018) confirmed that eutrophication levels can strongly favour perennial seagrass species and, to the contrary, fast-growing macroalgae in oligotrophic and eutrophic waters, respectively.

4.3. Influence of biological activity on diurnal water pCO_2 dynamics

At our studied continuum stations (*a*, *b*, *c* and *d*), negative correlations between water pCO_2 and DO, associated with large oxygen saturation ranges and strong $NpCO_2$ effects on the measured pCO_2 values, were calculated at the diurnal scale, particularly at the artificial marsh stations (Figs. 5 and 6). It partly demonstrates the strong biological influence of both autotrophic (macrophytes and phytoplankton) and heterotrophic (bacteria) organisms on the diurnal dynamics of inorganic C. Dai et al. (2009) confirmed that C biogeochemical processes

745 in coastal environments such as the Fier d'Ars system are generally controlled by non-
746 temperature effects (biological and tidal effects) compared to more open systems like the
747 Atlantic Ocean. Several studies have shown a major biological control on diurnal pCO_2
748 variations in coastal systems such as the temperate Bay of Brest (France; Bozec et al. 2011),
749 the Arcachon tidal flat (France; Polsenaere et al. 2022), a shallow subtropical estuary in Tampa
750 Bay (USA; Yates et al. 2007) and the tropical coastal embayment at Guanabara Bay (Brazil;
751 Cotovicz Jr. et al. 2015). At the Fier d'Ars estuary (station *a*) in spring and summer 2018, we
752 calculated non-significant correlations between the measured pCO_2 and estimated TA values
753 and between the measured pH and estimated TA values. We also calculated significant positive
754 correlations between the measured DO and pH values ($R^2 = 0.75$ and $R^2 = 0.50$, respectively; p
755 < 0.0001; regressions not shown) and between the measured DO and pCO_2 values ($R^2 = 0.86$
756 and $R^2 = 0.91$, respectively; $p < 0.0001$; regressions not shown). These results confirmed the
757 significant control of the photosynthesis *vs.* respiration balance and the weaker influence of the
758 carbonate system on diurnal pCO_2 variations as shown by Yates et al. (2007) in Tampa Bay. At
759 station *c*, in spring and summer 2019 during the day, macroalgae CO_2 uptake induced large CO_2
760 undersaturation periods associated with high oxygen saturations (> 170%) in the water column;
761 during the night, macroalgae respiration consumed large oxygen quantities and therefore very
762 low oxygen saturations were observed (< 60%; Fig. 5). In winter 2020, during the marsh
763 confinement, the highest diurnal variations in water pCO_2 were recorded with a pCO_2 decrease
764 of 386 ppmv during the day and an increase of 119 ppmv during the night; again, this may
765 confirm significant photosynthesis and respiration processes in these shallow marsh waters
766 (Fig. 5). By comparison, in a *Zostera marina* meadow (South Bay, USA) in spring and summer
767 2015, Berg et al. (2019) measured similar diurnal fluctuations of water pCO_2 that were directly
768 controlled by seagrass metabolism with diurnal ranges of 528 and 603 ppmv in late April and

late June, respectively. At station *d*, during periods when the lock was closed, the temperature and non-temperature effects on water pCO_2 were 9 and 115 ppmv, respectively in autumn 2019 and 34 and 134 ppmv, respectively in winter 2020 showing also an influence of biological processes on the diurnal pCO_2 dynamics (Fig. 6). In tidal estuaries and salt marshes, diurnal variations in water pCO_2 due to biological influence must therefore be measured and better accounted for CO_2 budget studies to avoid overestimating their CO_2 sink potential through daytime pCO_2 measurements only (Cotovicz Jr. et al. 2015).

4.4. Biogeochemical station interconnections through tidal advection

Along the studied aquatic continuums, horizontal advection can significantly control water pCO_2 variations at the tidal scale. As seen during the present study, flooding of the *Filiere W* shelf waters induced a salinity increase and a decrease in winter and from spring to autumn, respectively, at stations *a*, *b*, *c* and *d* along with significant water pCO_2 variations. For instance, at tidal stations (*a* and *b*) in spring and summer during the day, flooding of the shelf waters created a significant decrease in water pCO_2 since the advected waters were CO_2 undersaturated compared with estuarine waters (Figs. 3 and 4). This observation was confirmed by significant negative correlations calculated between pCO_2 and water heights during this period, highlighting the strong control of tidal rhythm on the coastal waters pCO_2. Along the French Atlantic coast, Polsenaere et al. (2022) also showed a strong control of the tidal rhythm in the Arcachon lagoon with higher pCO_2 values measured at LT than at HT during each season in 2008 and 2009. Similarly, in the Sancti Petri Channel and its adjacent salt marshes, Burgos et al. (2018) recorded the highest and lowest pCO_2 values (1059 and 754 ppmv) at LT and HT, respectively. Even stronger tidal influences on in situ water pCO_2 (from 1380 to 4770 ppmv

792 between HT and LT) were observed by Borges (2003) in summer 2001 in a mangrove system
793 (Gaderu Creek). Interestingly, at station *a* in summer 2018, a significant water pCO_2 decrease
794 from 370 ppmv (15:00) to 267 ppmv (19:30) associated with an oxygen saturation increase
795 from 120 to 140% (characteristic of macrophyte biological activity) was observed in estuary
796 waters during a receding tide, certainly due to CO_2 undersaturated upstream waters from the
797 productive artificial salt marsh waters (Fig. 3). In spring and summer, marsh waters at station *c*
798 were largely CO_2 undersaturated due to the high primary production of macroalgae and in
799 particular, the long water residence times; however, more CO_2-enriched water inflows from
800 stations *Filiere W*, *a* and *b* instantly produced significant water pCO_2 increases at this marsh
801 station (Fig. 5). Therefore, in each season (except at station *d* in autumn and winter), variations
802 in marsh water pCO_2 at the tidal scale were dependent on the biogeochemical state of the
803 advected waters downstream from the shelf, estuary and channel with respect to CO_2 saturation.

804

805 **4.5. Metabolism assessment of the Fier d'Ars continuums**

806 Over the year 2018, the Fier d'Ars estuary (station *a*) behaved on average as a yearly CO_2
807 sink close to the atmospheric equilibrium, although a significant sink was measured in the
808 spring (Table 3) due to potential phytoplankton blooms occurring in coastal waters (see
809 previous sections in the Discussion). Conversely, over the same meteorological periods, the
810 channel (station *b*) was a net annual source from its turbid waters to the atmosphere due to
811 several oversaturation periods, particularly in winter, characterized by the highest wind speed
812 and CO_2 exchange coefficient values (Table 3 and Fig. 8). Over the subtidal Bay of Brest, Bozec
813 et al. (2011) estimated slightly higher air-water FCO_2 values ranging from -0.38 to 0.01 mmol
814 m^{-2} h^{-1} during spring/summer and from 0.04 to 0.91 mmol m^{-2} h^{-1} during autumn/winter (Table

3). In the Arcachon tidal lagoon (similar to our stations *a* and *b*) using the same 24-hour cycle approach, an annual air-water FCO_2 was estimated to be 0.27 ± 0.22 mmol m^{-2} h^{-1}, the highest and the lowest CO_2 degassing values recorded in September and January 2009, respectively (Polsenaere et al. 2022). In the present study, rewilded artificial salt marsh waters (station *c*) behaved as a yearly source of atmospheric CO_2 when macroalgae degradation and mineralization processes produced strong CO_2 effluxes to the atmosphere, as in autumn 2019 (Fig. 8; see previous sections in the Discussion). On the contrary, the working artificial salt marsh (station *d*) behaved as the largest yearly CO_2 sink particularly favoured by inexistent tidal variations (lock closure) in the absence of salt-farming activities (from fall to winter; Fig. 8). Within the Duplin River salt marsh-estuary coastal ecosystem, both channel and marsh waters degassed CO_2 to the atmosphere and, unlike our studied stations, the highest and lowest sources were recorded in summer (5.50 and 3.90 mmol m^{-2} h^{-1} from channel and marsh waters, respectively) and in winter (0.70 and 0.60 mmol m^{-2} h^{-1} from channel and marsh waters, respectively), respectively (Wang et al. 2018). Overall, the whole Duplin system emits more CO_2 into atmosphere than the Fier d'Ars system, probably due to its more intense estuarine heterotrophic metabolism.

In autumn, the lack of significant variations in wind speeds between stations *a* and *b* in 2018 and between stations *c* and *d* in 2019, whereas atmospheric CO_2 exchanges significantly changed, highlighting the predominance of air-water CO_2 gradients in the control of CO_2 flux directions either as a sink or a source (Table 3). However, at the seasonal scale, the turbulence processes measured at the air-water interface also played an important role in flux variability and magnitude; for instance, at station *a* between spring and summer and at station *b* between winter and summer, wind speed variability produced significant FCO_2 variations although no significant air-water CO_2 gradients were measured (Table 3). Atmospheric exchanges in

839 marshes are therefore dependent on the CO_2 saturation state of the water column (air-water
840 gradient) considering that the wind only acts as a driver of the flux (Polsenaere et al. 2022).
841 Moreover, the (site specific) methodological calculations and associated differences chosen for
842 the exchange coefficient parameterizations (higher fluxes with RC01 than with W92 methods;
843 Table 3) may produce even more contrasts in the estimated air-water FCO_2 values (Cotovicz
844 Jr. et al. 2015, Polsenaere et al. 2022).

845 By scaling-up and considering stations *a* and *b* together along the continuum (estuary and
846 channel), an annual source of atmospheric CO_2 of 7.3 g C m^{-2} yr^{-1} was calculated in 2018. The
847 rewilded artificial salt marsh (station *c*) emitted 17.5 g C m^{-2} yr^{-1} (702.0 kg C yr^{-1}) to the
848 atmosphere, when the working artificial marsh (station *d*) absorbed 97.7 g C m^{-2} yr^{-1} (828.6 kg
849 C yr^{-1}) from the atmosphere. A larger scale study of C along three shelf – estuary – tidal wetland
850 continuums on the Atlantic coast of the United States also showed strong spatial variations in
851 atmospheric CO_2 exchanges with CO_2 uptake for wetland and shelf waters of 5.3 ± 1.5 and 4.0
852 ± 0.7 Tg C yr^{-1}, respectively and a CO_2 source from estuarine waters of 4.2 ± 1.7 Tg C yr^{-1}
853 (Najjar et al. 2018). During our study, contrasting stations along the continuums were sampled
854 via seasonal 24-hour cycles to estimate the air-water CO_2 exchanges. However, longer seasonal
855 measurement periods up to several days would be more representative of the strong temporal
856 variability in k_{660}, water pCO_2 and other biogeochemical parameters. At the Bossys perdus salt
857 marsh (station *e*; Fig. 1), another flux methodology using the atmospheric EC technique was
858 deployed to continuously measure year-round in situ CO_2 fluxes at the ecosystem scale under
859 real field conditions. Over the year 2020, this preserved salty meadow fixed 483 g C m^{-2} yr^{-1}
860 from the atmosphere, which is much higher than the studied artificial salt marshes indicating a
861 potential stronger atmospheric CO_2 sink in tidal salt marshes (Mayen et al. in prep.). However,
862 it is also important to study the whole marsh metabolism taking terrestrial and aquatic

compartments into account and distinguishing their respective contributions to atmospheric fluxes and the regional C budgets of the associated marshes. To do this, we measured the atmospheric CO_2 exchanges at the ecosystem scale at both the water-air and soil-air interfaces, biogeochemical parameters of the channel column water, metabolic balance of planktonic communities and horizontal C export during seasonal 24-hour cycles to be more integrative from a C budget point of view over the salt marshes (Mayen et al. in prep.).

Acknowledgements

I would like to thank the Scientific direction of Ifremer (French research institute for exploitation of the sea) for financing my PhD thesis (2020-2023). We would like to sincerely thank the oyster farmers for their help with taking samples at station *a*, Julien Gernigon from the Lilleau des Niges NNR (LPO) and Brice Collonier from the Loix Ecomuseum on Ré Island for their help and the information given at stations *b*, *c*, *d* and *e*. We are grateful to Jean-Michel Chabirand and James Grizon for their help with deploying the field sensors and to Philippe Geairon for his map making. We would also like thank Quentin Ternon, Gabriel Devique and Jonathan Deborde for their help in the field. This paper is a contribution to the ANR-PAMPAS project (Agence Nationale de la Recherche « Evolution de l'identité patrimoniale des marais des Pertuis Charentais en réponse à l'aléa de submersion marine », ANR-18-CE32-0006), the CNRS-INSU LEFE DYCIDEMAIM project (DYnamique du Carbone aux Interfaces D'Échange des MArais tIdaux teMpérés) and to the Master (M1, M2) and PhD works of Jérémy Mayen funded by IFREMER.

886 Abril G, Commarieu M-V, Sottolichio A, Bretel P, Guérin F (2009) Turbidity limits gas
887 exchange in a large macrotidal estuary. Estuarine, Coastal and Shelf Science 83:342–
888 348.

889 Adam P (2019) Salt Marsh Restoration. In: *Coastal Wetlands*. Elsevier, p 817–861

890 Aminot A, Kerouel R (2004). Hydrologie des écosystèmes marins. Paramètres et analyses. Ed.
891 Ifremer

892 Amorocho J, DeVries JJ (1980) A new evaluation of the wind stress coefficient over water
893 surfaces. J Geophys Res 85:433.

894 Artigas F, Shin JY, Hobble C, Marti-Donati A, Schäfer KVR, Pechmann I (2015) Long term
895 carbon storage potential and CO_2 sink strength of a restored salt marsh in New Jersey.
896 Agricultural and Forest Meteorology 200:313–321.

897 Aufdenkampe AK, Mayorga E, Raymond PA, Melack JM, Doney SC, Alin SR, Aalto RE, Yoo
898 K (2011) Riverine coupling of biogeochemical cycles between land, oceans, and
899 atmosphere. Frontiers in Ecology and the Environment 9:53–60.

900 Bade DL (2009) Gas Exchange at the Air–Water Interface. In: *Encyclopedia of Inland Waters*.
901 Elsevier, p 70–78

902 Baldocchi DD (2003) Assessing the eddy covariance technique for evaluating carbon dioxide
903 exchange rates of ecosystems: past, present and future: CARBON BALANCE and
904 EDDY COVARIANCE. Global Change Biology 9:479–492.

905 Baldocchi DD, Hincks BB, Meyers TP (1988) Measuring Biosphere-Atmosphere Exchanges
906 of Biologically Related Gases with Micrometeorological Methods. Ecology 69:1331–
907 1340.

908 Bauer JE, Cai W-J, Raymond PA, Bianchi TS, Hopkinson CS, Regnier PAG (2013) The
909 changing carbon cycle of the coastal ocean. Nature 504:61–70.

910 Bel Hassen M (2001) Spatial and Temporal Variability in Nutrients and Suspended Material
911 Processing in the Fier d'Ars Bay (France). Estuarine, Coastal and Shelf Science 52:457–
912 469.

913 Belin C, Soudant D, Amzil Z (2021) Three decades of data on phytoplankton and phycotoxins
914 on the French coast: Lessons from REPHY and REPHYTOX. Harmful Algae
915 102:101733.

916 Berg P, Delgard ML, Polsenaere P, McGlathery KJ, Doney SC, Berger AC (2019) Dynamics
917 of benthic metabolism, O_2, and pCO_2 in a temperate seagrass meadow. Limnol
918 Oceanogr 64:2586–2604.

919 Borges AV (2003) Atmospheric CO_2 flux from mangrove surrounding waters. Geophys Res
920 Lett 30:1558.

921 Borges AV, Abril G (2011) Carbon Dioxide and Methane Dynamics in Estuaries. In: *Treatise*
922 *on Estuarine and Coastal Science*. Elsevier, p 119–161

923 Borges AV, Delille B, Frankignoulle M (2005) Budgeting sinks and sources of CO_2 in the
924 coastal ocean: Diversity of ecosystems counts: COASTAL CO_2 SINKS AND
925 SOURCES. Geophys Res Lett 32.

926 Bozec Y, Merlivat L, Baudoux A-C, Beaumont L, Blain S, Bucciarelli E, Danguy T,
927 Grossteffan E, Guillot A, Guillou J, Répécaud M, Tréguer P (2011) Diurnal to inter-
928 annual dynamics of pCO_2 recorded by a CARIOCA sensor in a temperate coastal
929 ecosystem (2003–2009). Marine Chemistry 126:13–26.

930 Burgos M, Ortega T, Forja J (2018) Carbon Dioxide and Methane Dynamics in Three Coastal
931 Systems of Cadiz Bay (SW Spain). Estuaries and Coasts 41:1069–1088.

932 Cai W-J (2011) Estuarine and Coastal Ocean Carbon Paradox: CO_2 Sinks or Sites of Terrestrial
933 Carbon Incineration? Annu Rev Mar Sci 3:123–145.

934 Champion E, Gernigon J, Lemesle J-C, Terrisse J, Maisonhaute S (2012) 3ème Plan de gestion
935 2013-2017 de la réserve naturelle nationale de Lilleau des Niges.

936 Chmura GL, Anisfeld SC, Cahoon DR, Lynch JC (2003) Global carbon sequestration in tidal,
937 saline wetland soils. Global Biogeochem Cycles 17(4), 1111,
938 doi:10.1029/2002GB001917, 2003.

939 Cloern JE, Foster SQ, Kleckner AE (2014) Phytoplankton primary production in the world's
940 estuarine-coastal ecosystems. Biogeosciences 11:2477–2501.

941 Coignot E, Polsenaere P, Soletchnik P, Le Moine O, Souchu P, Joyeux E, Le Roy Y, Guéret J-
942 P, Froud L, Gallais R, Chourré E, Chaigneau L (2020) Variabilité spatio-temporelle des
943 nutriments et du carbone et flux associés le long d'un continuum terrestre-aquatique
944 tempéré (Marais poitevin – Baie de l'Aiguillon – Pertuis Breton). Ifremer.

945 Cole JJ, Prairie YT, Caraco NF, McDowell WH, Tranvik LJ, Striegl RG, Duarte CM,
946 Kortelainen P, Downing JA, Middelburg JJ, Melack J (2007) Plumbing the Global
947 Carbon Cycle: Integrating Inland Waters into the Terrestrial Carbon Budget.
948 Ecosystems 10:172–185.

949 Cotovicz Jr. LC, Knoppers BA, Brandini N, Costa Santos SJ, Abril G (2015) A strong CO_2 sink
950 enhanced by eutrophication in a tropical coastal embayment (Guanabara Bay, Rio de
951 Janeiro, Brazil). Biogeosciences 12:6125–6146.

952 Crosswell JR, Anderson IC, Stanhope JW, Dam BV, Brush MJ, Ensign S, Piehler MF, McKee
953 B, Bost M, Paerl HW (2017) Carbon budget of a shallow, lagoonal estuary:
954 Transformations and source-sink dynamics along the river-estuary-ocean continuum.
955 Limnology and Oceanography 62:S29–S45.

956 Dai M, Lu Z, Zhai W, Chen B, Cao Z, Zhou K, Cai W-J, Chenc C-TA (2009) Diurnal variations
957 of surface seawater pCO_2 in contrasting coastal environments. Limnol Oceanogr
958 54:735–745.

959 Dai M, Su J, Zhao Y, Hofmann EE, Cao Z, Cai W-J, Gan J, Lacroix F, Laruelle GG, Meng F,
960 Müller JD, Regnier PAG, Wang G, Wang Z (2022) Carbon Fluxes in the Coastal Ocean:
961 Synthesis, Boundary Processes, and Future Trends. Annu Rev Earth Planet Sci 50:593–
962 626.

963 Deegan LA, Johnson DS, Warren RS, Peterson BJ, Fleeger JW, Fagherazzi S, Wollheim WM
964 (2012) Coastal eutrophication as a driver of salt marsh loss. Nature 490:388–392.

965 Dickson AG, Millero FJ (1987) A comparison of the equilibrium constants for the dissociation
966 of carbonic acid in seawater media. *Deep-Sea Research* 34: 1733–1743.

967 Dickson AG (1990) Standard potential of the reaction: AgCl(s) + 1⁄2H2(g) = Ag(s) + HCl(aq),
968 and the standard acidity constant of the ion HSO_4^- in synthetic sea water from 273.15
969 to 318.15 K. *Journal of Chemical Thermodynamics* 22: 113–127.

970 Duarte CM, Cebrián J (1996) The fate of marine autotrophic production. Limnol Oceanogr
971 41:1758–1766.

972 Dürr HH, Laruelle GG, van Kempen CM, Slomp CP, Meybeck M, Middelkoop H (2011)
973 Worldwide Typology of Nearshore Coastal Systems: Defining the Estuarine Filter of
974 River Inputs to the Oceans. Estuaries and Coasts 34:441–458.

975 Forbrich I, Giblin AE (2015) Marsh-atmosphere CO_2 exchange in a New England salt marsh. J
976 Geophys Res Biogeosci 120:1825–1838.

977 Frankignoulle M, Abril G, Borges A, Bourge I, Canon C, Delille B, Libert E, Théate J-M (1998)
978 Carbon Dioxide Emission from European Estuaries. Science, New Series 282:434–436.

979 Gattuso J-P, Frankignoulle M, Wollast R (1998) CARBON AND CARBONATE
980 METABOLISM IN COASTAL AQUATIC ECOSYSTEMS. Annu Rev Ecol Syst
981 29:405–434.

982 Gouazé M (2019) Étude du couple benthos-pélagos dans les marais littoraux et rétro-littoraux
983 de Charente Maritime. La Rochelle Université, La Rochelle.

984 Gu J, Luo M, Zhang X, Christakos G, Agusti S, Duarte CM, Wu J (2018) Losses of salt marsh
985 in China: Trends, threats and management. Estuarine, Coastal and Shelf Science
986 214:98–109.

987 Hill R, Bellgrove A, Macreadie PI, Petrou K, Beardall J, Steven A, Ralph PJ (2015) Can
988 macroalgae contribute to blue carbon? An Australian perspective: Can macroalgae
989 contribute to blue carbon? Limnol Oceanogr 60:1689–1706.

990 Jähne B, Münnich KO, Bösinger R, Dutzi A, Huber W, Libner P (1987) On the parameters
991 influencing air-water gas exchange. J Geophys Res 92:1937.

992 Jiang L-Q, Cai W-J, Wang Y (2008) A comparative study of carbon dioxide degassing in river-
993 and marine-dominated estuaries. Limnol Oceanogr 53:2603–2615.

994 Krause-Jensen D, Duarte CM (2016) Substantial role of macroalgae in marine carbon
995 sequestration. Nature Geosci 9:737–742.

996 Le Fur I, De Wit R, Plus M, Oheix J, Simier M, Ouisse V (2018) Submerged benthic
997 macrophytes in Mediterranean lagoons: distribution patterns in relation to water
998 chemistry and depth. Hydrobiologia 808:175–200.

999 Lê S, Josse J, Husson F (2008) FactoMineR: An *R* Package for Multivariate Analysis. J Stat
1000 Soft 25.

1001 Lee K, Kim T-W, Byrne RH, Millero FJ, Feely RA, Liu Y-M (2010) The universal ratio of
1002 boron to chlorinity for the North Pacific and North Atlantic oceans. Geochimica et
1003 Cosmochimica Acta 74:1801–1811.

1004 Lewis E, Wallace D (1998) Program developed for CO_2 system calculations. *Carbon dioxide*
1005 *information analysis center. Oak Ridge National Laboratory*

1006 Macreadie PI, Nielsen DA, Kelleway JJ, Atwood TB, Seymour JR, Petrou K, Connolly RM,
1007 Thomson AC, Trevathan-Tackett SM, Ralph PJ (2017) Can we manage coastal
1008 ecosystems to sequester more blue carbon? 8.

1009 Maher DT and Eyre BD (2012) Carbon budgets for three autotrophic Australian estuaries:
1010 Implications for global estimates of the coastal air-water CO_2 flux, Global Biogeochem.
1011 Cycles, 26, GB1032, doi:10.1029/2011GB004075

1012 Mcleod E, Chmura GL, Bouillon S, Salm R, Björk M, Duarte CM, Lovelock CE, Schlesinger
1013 WH, Silliman BR (2011) A blueprint for blue carbon: toward an improved
1014 understanding of the role of vegetated coastal habitats in sequestering CO_2. Frontiers in
1015 Ecology and the Environment 9:552–560.

1016 Mehrbach C, Culberson CH, Hawley JE, Pytkowicz RM (1973) Measurement of the Apparent
1017 Dissociation Constants of Carbonic Acid in Seawater at Atmospheric Pressure.
1018 Limnology and Oceanography 18:897–907.

1019 Najjar RG, Herrmann M, Alexander R, Boyer EW, Burdige DJ, Butman D, Cai W -J., Canuel
1020 EA, Chen RF, Friedrichs MAM, Feagin RA, Griffith PC, Hinson AL, Holmquist JR,
1021 Hu X, Kemp WM, Kroeger KD, Mannino A, McCallister SL, McGillis WR, Mulholland
1022 MR, Pilskaln CH, Salisbury J, Signorini SR, St-Laurent P, Tian H, Tzortziou M, Vlahos
1023 P, Wang ZA, Zimmerman RC (2018) Carbon Budget of Tidal Wetlands, Estuaries, and
1024 Shelf Waters of Eastern North America. Global Biogeochem Cycles 32:389–416.

1025 Newton C, Thornber C (2013) Ecological Impacts of Macroalgal Blooms on Salt Marsh
1026 Communities. Estuaries and Coasts 36:365–376.

1027 Palacios MM, Trevathan-Tackett SM, Malerba ME, Macreadie PI (2021) Effects of a nutrient
1028 enrichment pulse on blue carbon ecosystems. Marine Pollution Bulletin 165:112024.

1029 Paticat F (2007) Flux et usages de l'eaude mer dans les marais salés endigués Charentais: Cas
1030 du marais salé endigué de l'île de Ré. Thèse, Nantes

1031 Polsenaere P (2011) Echange de CO_2 atmospherique dans la lagune d'Arcachon et relations
1032 avec le métabolisme intertidal. Thèse, Bordeaux

1033 Polsenaere P, Lamaud E, Lafon V, Bonnefond J-M, Bretel P, Delille B, Deborde J, Loustau D,
1034 Abril G (2012) Spatial and temporal CO_2 exchanges measured by Eddy Covariance over
1035 a temperate intertidal flat and their relationships to net ecosystem production.
1036 Biogeosciences 9:249–268.

1037 Polsenaere P, Deborde J, Detandt G, Vidal LO, Pérez MAP, Marieu V, Abril G (2013) Thermal
1038 enhancement of gas transfer velocity of CO_2 in an Amazon floodplain lake revealed by
1039 eddy covariance measurements: GAS TRANSFER VELOCITY IN AN AMAZON
1040 LAKE. Geophys Res Lett 40:1734–1740.

1041 Polsenaere P, Soletchnik P, Le Moine O, Gohin F, Robert S, Pépin J-F, Stanisière J-Y, Dumas
1042 F, Béchemin C, Goulletquer P (2017) Potential environmental drivers of a regional blue
1043 mussel mass mortality event (winter of 2014, Breton Sound, France). Journal of Sea
1044 Research 123:39–50.

1045 Polsenaere P, Delille B, Poirier D, Charbonnier C, Deborde J, Mouret A, Abril G (2022)
1046 Seasonal, Diurnal, and Tidal Variations of Dissolved Inorganic Carbon and pCO_2 in
1047 Surface Waters of a Temperate Coastal Lagoon (Arcachon, SW France). Estuaries and
1048 Coasts.

1049 Raven J (2018) Blue carbon: past, present and future, with emphasis on macroalgae. Biol Lett
1050 14:20180336.

1051 Raymond PA, Cole JJ (2001) Gas Exchange in Rivers and Estuaries: Choosing a Gas Transfer
1052 Velocity. Estuaries 24:312.

1053 REPHY – French Observation and Monitoring program for Phytoplankton and Hydrology in
1054 coastal waters (2021). REPHY dataset - French Observation and Monitoring program
1055 for Phytoplankton and Hydrology in coastal waters. Metropolitan data. SEANOE.
1056 https://doi.org/10.17882/47248

1057 Ribas-Ribas M, Gómez-Parra A, Forja JM (2011) Air–sea CO_2 fluxes in the north-eastern shelf
1058 of the Gulf of Cádiz (southwest Iberian Peninsula). Marine Chemistry 123:56–66.

1059 Savelli R, Bertin X, Orvain F, Gernez P, Dale A, Coulombier T, Pineau P, Lachaussée N,
1060 Polsenaere P, Dupuy C, Le Fouest V (2019) Impact of Chronic and Massive
1061 Resuspension Mechanisms on the Microphytobenthos Dynamics in a Temperate
1062 Intertidal Mudflat. J Geophys Res Biogeosci 124:3752–3777.

1063 Schäfer KVR, Tripathee R, Artigas F, Morin TH, Bohrer G (2014) Carbon dioxide fluxes of an
1064 urban tidal marsh in the Hudson-Raritan estuary: Carbon dioxide fluxes of an wetland.
1065 J Geophys Res Biogeosci 119:2065–2081.

1066 Soletchnik P, Polsenaere P, Le Moine O, Guesdon S, Bechemin C (2014) Interactions between
1067 river freshwater inputs and the shellfish farming (oysters and mussels) in the Pertuis
1068 Charentais (France).

1069 Stanisiere J-Y, Dumas F, Plus M, Maurer D, Robert S (2006) Hydrodynmaic characterization
1070 of a semi-enclosed coastal system : Marennes Oleron (France) basin.

1071 Takahashi T, Sutherland SC, Sweeney C, Poisson A, Metzl N, Tilbrook B, Bates N,
1072 Wanninkhof R, Feely RA, Sabine C, Olafsson J, Nojiri Y (2002) Global sea–air CO_2
1073 flux based on climatological surface ocean pCO_2, and seasonal biological and
1074 temperature effects. Deep Sea Research Part II: Topical Studies in Oceanography
1075 49:1601–1622.

1076 Teichberg M, Fox SE, Olsen YS, Valiela I, Martinetto P, Iribarne O, Muto EY, Petti MAV,
1077 Corbisier TN, Soto-Jiménez M, Páez-Osuna F, Castro P, Freitas H, Zitelli A,
1078 Cardinaletti M, Tagliapietra D (2010) Eutrophication and macroalgal blooms in
1079 temperate and tropical coastal waters: nutrient enrichment experiments with *Ulva* spp.
1080 Global Change Biology 16:2624–2637.

1081 Ternon Q, Polsenaere P, Le Fouest V, Favier J-B, Philippine O, Chabirand J-M, Grizon J,
1082 Dupuy C (2018) Étude des pressions partielles et flux de CO_2 au sein de la Communauté
1083 d'Agglomération de La Rochelle. 32.

Tobias C, Neubauer SC (2019) Salt Marsh Biogeochemistry—An Overview. In: *Coastal Wetlands*. Elsevier, p 539–596

Tortajada S (2011) De l'étude du fonctionnement des réseaux trophiques planctoniques des marais de Charente Maritime vers la recherche d'indicateurs. Thèse, Université La Rochelle, La Rochelle

Tortajada S, David V, Brahmia A, Dupuy C, Laniesse T, Parinet B, Pouget F, Rousseau F, Simon-Bouhet B, Robin F-X (2011) Variability of fresh- and salt-water marshes characteristics on the west coast of France: A spatio-temporal assessment. Water Research 45:4152–4168.

Van Dam B, Polsenaere P, Barreras-Apodaca A, Lopes C, Sanchez-Mejia Z, Tokoro T, Kuwae T, Loza LG, Rutgersson A, Fourqurean J, Thomas H (2021) Global Trends in Air-Water CO_2 Exchange Over Seagrass Meadows Revealed by Atmospheric Eddy Covariance. Global Biogeochem Cycles 35.

Vandermeirsch F (2012) ÉTAT PHYSIQUE ET CHIMIQUE Caractéristiques physiques.

Wang SR, Di Iorio D, Cai W, Hopkinson CS (2018) Inorganic carbon and oxygen dynamics in a marsh-dominated estuary. Limnol Oceanogr 63:47–71.

Wang ZA, Cai W-J (2004) Carbon dioxide degassing and inorganic carbon export from a marsh-dominated estuary (the Duplin River): A marsh CO_2 pump. Limnol Oceanogr 49:341–354.

Wang ZA, Kroeger KD, Ganju NK, Gonneea ME, Chu SN (2016) Intertidal salt marshes as an important source of inorganic carbon to the coastal ocean. Limnol Oceanogr 61:1916–1931.

1106 Wanninkhof R (1992) Relationship between wind speed and gas exchange over the ocean. J
1107 Geophys Res 97:7373.

1108 Wei, T., & Simko, V. (2017). *R package "corrplot": Visualization of a Correlation Matrix*.
1109 https://github.com/taiyun/corrplot

1110 Weiss RF (1974) Carbon dioxide in water and seawater: the solubility of a non-ideal gas.
1111 Marine Chemistry 2:203–215.

1112 Yates KK, Dufore C, Smiley N, Jackson C, Halley RB (2007) Diurnal variation of oxygen and
1113 carbonate system parameters in Tampa Bay and Florida Bay. Marine Chemistry
1114 104:110–124.

1115

1116